Photosynth Res
DOI 10.1007/s11120-009-9487-2

TECHNICAL COMMUNICATION

A new setup for in vivo fluorescence imaging of photosynthetic activity

Xenie Johnson · Guillaume Vandystadt · Sandrine Bujaldon · Francis-André Wollman · Rémi Dubois · Pierre Roussel · Jean Alric · Daniel Béal

Received: 2 June 2009 / Accepted: 3 August 2009

Abstract Here, we describe a new imaging setup able to assess in vivo photosynthetic activity. The system specifically measures time-resolved chlorophyll fluorescence in response to light. It is composed of a fast digital camera equipped with a wide-angle lens for the analysis of samples up to 10 × 10 cm, i.e. entire plants or petri dishes. In the choice of CCD, we have opted for a 12-bits high frame rate [150 fps (frames per second)] at the expense of definition (640 × 480 pixels). Although the choice of digital camera is always a compromise between these two related features, we have designed a flexible system allowing the fast sampling of images (down to 100 µs) with a maximum spatial resolution. This image readout system, synchronized with actinic light and saturating pulses, allows a precise determination of F_0 and F_M, which is required to monitor PSII activity. This new imaging system, together with image processing techniques, is useful to investigate the heterogeneity of photosynthetic activity within leaves or to screen large numbers of unicellular algal mutant colonies to identify those with subtle changes in photosynthetic electron flow.

Keywords Chlorophyll fluorescence · Imaging techniques · Screening of algal colonies

Abbreviations

CCD	Charge-coupled device
Pixel	Picture element
LED	Light-emitting diode
cyt	Cytochrome
PSI	Photosystem I
PSII	Photosystem II
PQ	Plastoquinone
PQH_2	Plastoquinol

Introduction

Chlorophyll fluorescence detection is a non-invasive technique for the imaging of photosynthetic fluxes (see Baker 2008 for a recent review). A fraction of the light absorbed by the biological material is not used for energy conversion, but reemitted as fluorescence photons: the fluorescence signal is therefore complementary to the photosynthetic activity. The time course of this fluorescence signal in response to light excitation, known as the variable fluorescence (F_V), provides rich information for interpretation of electron transfer at the molecular level. Higher plants and unicellular green algae such as *Chlamydomonas reinhardtii* possess chloroplasts with thylakoid membranes containing the photosystems PSI and PSII connected to each other by the cytochrome b_6f complex. PSI can give rise to variable

Electronic supplementary material The online version of this article (doi:10.1007/s11120-009-9487-2) contains supplementary material, which is available to authorized users.

X. Johnson · G. Vandystadt · S. Bujaldon · F.-A. Wollman · J. Alric · D. Béal
Institut de Biologie Physico-Chimique, UMR 7141, CNRS et Université Pierre et Marie Curie (Paris VI), 13 rue Pierre et Marie Curie, 75005 Paris, France

R. Dubois · P. Roussel
Ecole Supérieure de Physique et de Chimie Industrielles de la ville de Paris (ESPCI-Paristech), Laboratoire d'Electronique (UMR CNRS 7084), 75231 Paris Cedex 05, France

X. Johnson · R. Dubois · P. Roussel · J. Alric (✉)
Fondation Pierre-Gilles de Gennes pour la Recherche, 29 rue d'Ulm, 75005 Paris, France
e-mail: jean.alric@ibpc.fr

Published online: 21 August 2009

fluorescence under very low-potential conditions, but under standard conditions PSII is the only contributor to variable fluorescence. Basically, when the donor side of PSII is intact, the variable fluorescence signal reflects the redox state of the secondary electron acceptor Q_A even though the relationship is not strictly linear, see Cuni et al. (2004). The midpoint potential of the Q_A/Q_A^- redox couple is about −30 mV and the midpoint potential of PQ/PQH_2 is about +110 mV. This leads to an equilibrium constant of ~100 between Q_A and the PQ pool and implies that the fluorescence signal is highly sensitive to weak changes in the redox state of the quinone pool when the reducing pressure (light intensity) is strong, i.e. when the pool is mostly reduced.

Chlorophyll fluorescence induction kinetics are thus a very rich observable of overall photosynthetic activity. In order to describe this activity, a few parameters should be defined: the fluorescence yield of the dark-adapted state (F_0, Q_A fully oxidized and PQ pool mostly oxidized), the maximum fluorescence yield obtained with saturating light (F_M, Q_A reduced and PQ pool fully reduced) and the steady-state fluorescence level (F_S). Since F_S is a steady state, its measurement is relatively easy, while the determination of transients F_0 and F_M requires an excellent time resolution (<1 ms). To our knowledge, commercial systems use cameras with a continuous readout of 30 (imaging PAM; Schreiber et al. 2007) or 50 (Handy FluorCam; Nedbal et al. 2000) frames per second (fps), with a pulse amplitude modulation (PAM) detection. This limitation in the repetition rate of the detection was previously due to CCD technology which does not allow maximizing both temporal and spatial resolutions: the higher the image definition, the longer the read out time. The high-performance camera used in our apparatus has a CCD with gated integration that allows for a variable exposure time. These features, together with a fitted illumination system, give a detection of F_0 and F_M in the range of 1 ms and down to 100 µs when requested.

Improving time resolution is not straightforward. In fluorescence measurements, like all photometric techniques, the sensitivity is limited by the number of photons which can be captured by the detector. Digital images are particularly subject to this limitation as the detector is fragmented in numerous picture elements (pixels) where an individual surface area is much smaller than the usual photodiode or photomultiplier. For kinetics measurements, the crucial parameter still remains light capture and thus the number of photons per time unit. The challenge is to increase time resolution without sacrificing sensitivity. It is a well-known trade off in photography and generally treated by increasing light intensity to compensate for a decrease in exposure time. This has an inherent limit when applied to the study of photosynthetic organisms since the light exposure is not without consequence to the photosynthetic process. In photosynthesis, the actinic effect of light is equal to the total number of photons absorbed by the sample throughout the entire period of illumination. Here, we describe a setup where the light used to probe the photosynthetic activity consists of short detection (<1 ms) pulses distinct from the actinic light used to induce changes in the photosynthetic process. Just as for photography, the principle of our detection of photosynthetic activity is to use a limited number of short light flashes or probe pulses. For each flash, the number of photons per time unit is maximized, but the total number of photons delivered throughout the period of the measurement remains within an acceptable range, i.e. non-actinic.

A similar spectroscopic technique has been successfully used to monitor in vivo fluorescence and absorbance changes in photosynthetic materials (Joliot et al. 1980). Here, we describe an advance in this technique which includes an imaging apparatus and which represents a significant improvement when compared to our previous setups (Bennoun and Béal 1997, 1998). We also present a typical application used to screen Chlamydomonas mutants deficient in b_6f complex accumulation to show the sensitivity of the measure to small changes in photosynthetic electron flow.

Materials and methods

Electronics

The imaging system (Fig. 1) includes a programmable digital delay generator similar to the commercialized version of JTS-10 (BioLogic, France). Such a programmable delay generator is used to trigger image acquisition (TTL) and illumination of the sample with light-emitting diodes (LEDs). The system has been upgraded by the addition of a high (voltage) power supply of 48 V providing a high current output to the LEDs. Twelve LEDs are connected in serial and each series of 12 are connected in parallel. Detection LEDs are supplied with short pulses of variable intensity (40 mA to 10 A) and duration (100 µs, 400 µs or 1 ms), synchronized to image acquisition. Actinic LEDs are supplied with various current ranges from 10 to 700 mA. The full power supply of the LEDs is achieved with eight rechargeable batteries (12 V) in series (100 V), providing a high-current output (20 A). A CMOS transistor is used to switch the power on the LEDs.

Illumination system

Such a high power supply is used to deliver a 250-ms saturating pulse of 2100 µE m^{-2} s^{-1} with a double ring of 156 green LEDs (Osram Platinium Dragon LTW5SN,

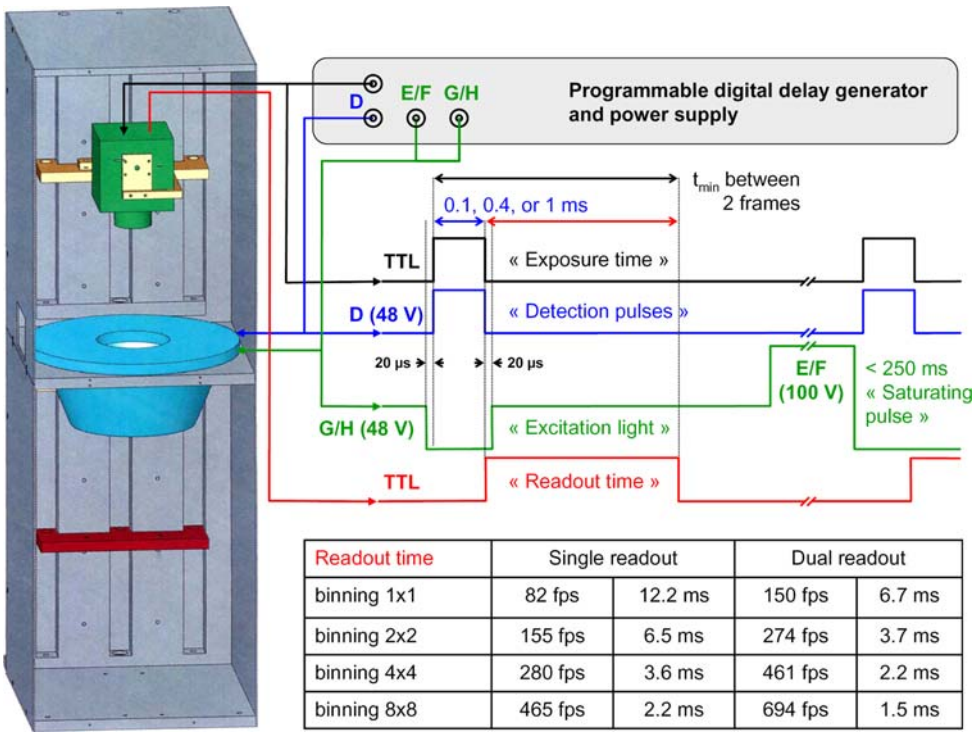

Readout time	Single readout		Dual readout	
binning 1x1	82 fps	12.2 ms	150 fps	6.7 ms
binning 2x2	155 fps	6.5 ms	274 fps	3.7 ms
binning 4x4	280 fps	3.6 ms	461 fps	2.2 ms
binning 8x8	465 fps	2.2 ms	694 fps	1.5 ms

Fig. 1 Schematic representation of the imaging setup. The imaging system is composed of an optical box containing (from the base upwards) a moveable sample holder (10 cm × 10 cm), illumination device with water-cooled ring of LEDs with a conical light condenser, and the CCD digital camera. The LEDs are driven by the digital delay generator. Information is sent to the computer to be processed and stored via video streaming, to complete the loop, sequence information is relayed to the digital pulse generator. A table of the readout speed in frames per second (fps) or time (in ms) is given as a function of the binning

520 nm). These green LEDs are also used for continuous light excitation of the sample with variable intensity (30–800 µE m^{-2} s^{-1}). The illumination system has an additional ring of 2 × 15 far-red LEDs (Roithner C11A1-740-60, 740 nm; Roithner C11A1-720-60, 720 nm) and 36 blue LEDs (Osram Platinium Dragon LBW5SN, 460 nm). Blue–green LEDs (10–2100 µE m^{-2} s^{-1}) are filtered through 2 mm thick Schott BG39 filters to cut off their far-red spectral emission. Far-red LEDs are filtered through 3 mm thick Schott RG715 filters to improve the specificity of PSI excitation. The LED rings are placed at a distance of 8 cm from the sample. An aluminium total internal reflectance cone is used for light condensation onto the sample. The system provides a homogenous illumination of different colours within a large area of 10 × 10 cm: the variations of light intensity do not exceed 5% along the *X*- and *Y*-axis of the image plane. Furthermore, the green LEDs illuminate the sample in the low-absorbance spectral region of chlorophyll; as a consequence, the green illumination deeply penetrates the sample and provides an homogenous illumination along the *Z*-axis (depth of field). Blue light, strongly absorbed by photosynthetic green organisms, is generally used for the pulse detection of fluorescence (see "Results and discussion" section below). Cool water is continuously flowed in the aluminium-made illumination system to avoid LEDs heating and temperature drift of their emitting wavelength. This water-cooling system also maintains a constant temperature of the sample, which is important for applications where an intense illumination can last several minutes (NPQ measurements).

Sample and camera holder

Translation stages are used to move the sample and the camera along the *Z*-axis. It accommodates enough room for large samples such as whole plants, while providing fine tuning of the working distance between the camera and the illuminated region of the sample. It allows the use of macro-lenses and extension tubes for close-up imaging.

Camera lens

A wide angle (17 mm) Xenon C-Mount lens (Schneider Optics, Germany) with high aperture (*f*/0.95) provides excellent luminosity for plane samples when the iris is open. Omega long-pass (>680 nm) dielectric filter 3RD680LP, placed in front of the objective, is used to select the chlorophyll fluorescence.

Digital camera

The CCD camera C93000-201 (Hamamatsu, Japan) has a quantum efficiency of more than 20% around 700 nm, which is the spectral region of chlorophyll fluorescence. The CCD has a readout noise of 20 electrons for a full well capacity of 20000 electrons, which is well suited for chlorophyll fluorescence applications (see below). The standard characteristics are 640 × 480 pixels, 12 bits output and 150 fps. For a given CCD, spatial resolution, dynamic range and readout speed are intrinsically linked because the improvement of the former two characteristics

will inevitably result in a slower frame rate. In spite of this, some additional features of this CCD camera improve its polyvalence and versatility. Two of them consist in accelerating the speed at the expense of spatial resolution: the sub-array and binning features. In the sub-array mode, only a selected area is readout from the CCD. In the binning mode, the signals of adjacent pixels of the CCD are summed (4 pixels in binning 2 × 2), without summing the readout noise. Both options, possibly used in combination, reduce the number of pixels to readout and increase the frame rate up to 1000 fps. Although very attractive for the study of transient signals, these kinetic improvements result in the degradation of the spatial resolution. In order to preserve the spatial resolution, while improving the time-resolution, we have taken advantage of the external trigger and the MHz electronic shutter, which allow a choice of the exposure time from 33 µs to 1 s, the readout time of the frame being <7 ms for 640 × 480 pixels.

Computer interface

A user-friendly PC interface has been developed in Visual Basic to control the programmable pulse generator and the camera interface. Two screens are used to display the numerous windows: LEDs intensities, parameters controlling the LEDs and the sampling, camera settings (trigger mode, gain, exposure time, binning), display of images/movies, display of the fluorescence kinetics picked in a region of interest, file outputs, etc. The data display is facilitated by the method of acquisition described above. Indeed, the sampling of only a few selected frames during fluorescence induction kinetics reduces the memory space required for data storage as well as the CPU time needed for data analysis.

Image processing and analysis

Typically, each frame consists of 640 × 480 pixels and the fluorescence kinetics over a 10-s period contains 30 frames. The aim of image processing is to extract relevant information from this large amount of data. It is clearly unrealistic to display the fluorescence kinetics curve for each pixel, thus some must be selected. This selection can be done manually through the computer interface described above: a pixel is selected on the displayed frame of a Petri dish and the associated kinetics curve is displayed. This approach can be used when only a few areas are to be analyzed and compared, but it becomes very tedious if many algal colonies are present on the same Petri dish.

This is the case when screening large numbers of mutant algal colonies. If the number of colonies per Petri dish reaches several hundred, an automatic procedure has to be implemented. This procedure locates the colonies on the brightest registered frame. It displays their location on the Petri dish and plots the associated fluorescence kinetics curves. It is then possible to trace a curve back to its location on the Petri dish. The selection of the colonies of interest, exhibiting an original behaviour, can be done directly by referring to the fluorescence curve, but additional information, which can considerably increase the ease of screening, can be extracted from these curves. Such parameters are, for example, the steady state fluorescence level (F_V), the first derivative of the dark-recovery or the presence of a notch on the initial rise of fluorescence. The representation of the colonies in two-dimensional spaces will help to locate outliers, whose original fluorescence behaviour may allow us to identify new mutants affected for metabolism and photosynthetic mechanisms.

Chlamydomonas strains and culture

Wild-type and mutant strains were grown in Tris–acetate phosphate medium (TAP), pH 7.2, at 25°C under continuous low light (300 lux). Mutants used in this work were QD3 (Kuras and Wollman 1994), C35V (de Vitry et al. 2004) and *ini*D (Chen et al. 1993).

Western blot analysis

Protein electrophoresis and immunoblotting were performed according to Kuras and Wollman (1994). Whole cell extracts were "broken" and analyzed on 12–18% polyacrylamide SDS gels in the presence of 8 M urea after loading (10 µg) on an equal chlorophyll basis. Proteins were transferred onto Hybond C extra membrane (Amersham Biosciences, UK), and ECL western blotting reagents (GE Healthcare, UK) were used to reveal the immunoreactive proteins. SUIV (1:5000 dilution)-probed blots were exposed on film (Kodak) for 2 min and CF0ß (1:40000 dilution) for 5 s. Signal was detected using the Typhoon TRIO phosphorimager (Amersham Biosciences, UK).

Results and discussion

Physical limitations

The theoretical (maximum) number of photons collected on the CCD can be calculated from:

(i) the light intensity delivered to the sample, for example, 50 µE m^{-2} s^{-1} = 50 × 10^{-6} × 6 × 10^{23} photons m^{-2} s^{-1},
(ii) the absorption of excitation light, about 90% of the photons absorbed,
(iii) the quantum yield of fluorescence in vivo, 3–5%,

(iv) the reabsorption of fluorescence emission, low in the far-red region of the spectrum, giving ~90% photons outgoing from the sample,
(v) the sample area corresponding to 1 pixel, about 200 × 200 μm = 4×10^{-8} m^2,
(vi) the solid angle from which this object is seen by a 16-mm diameter objective at 300 mm ($\pi \times 8 \times 8/300 \times 300$) over the total solid angle (4π), i.e. $\sim 1 \times 8 \times 10^{-4}$,
(vii) the loss in the fluorescence filter and the quantum yield of the CCD, ~10%,the exposure time, for example, 10 ms.

Such parameters account for the physical limitations of the experimental setup. It leads to about 900 photo-electrons per pixel, which is within the range of measurable signals at the level of the CCD (full well capacity of 20000 electrons). The camera seems, therefore, ideally suited for the chlorophyll fluorescence measurements: the 12 bits A/D converter would give $2^{12} \times 900/20000 = 184$ points over a full well capacity of 4096 points.

Brightness and time-resolution

We can test experimentally these theoretical values. When the exposure time is set to 10 ms, the fluorescence signal induced by an excitation of 50 μE m^{-2} s^{-1} of green light (520 nm) is $F_0 = 200$ points, i.e. in the expected order of magnitude. A similar fluorescence signal could be obtained with actinic blue light of weaker intensity (30 μE m^{-2} s^{-1}). It is merely due to a greater absorbance of blue light (470 nm). When blue light pulses are used as detectors, at maximum intensity but shorter duration (100 μs), a F_0 of 120 points is obtained. It means that the probe pulse, 100 times shorter than the integration time of 10 ms used above, has a maximum intensity of about $100 \times 30 \times 120/200 = 1800$ μE m^{-2} s^{-1}. Such a light intensity is saturating when applied continuously, but not significantly actinic when pulsed (100 μs). When applied during 1 ms, the actinic effect of the blue pulse becomes non-negligible, but it allows the full dynamic range of the detector to be used.

Signal-to-noise ratio

In this section, we would like to discuss the reasons for using the full well capacity of the CCD. The 12-bit A/D converter is well adapted since it covers the full well capacity (4096 points = 20000 photo-electrons) without being a limitation in the signal-to-noise ratio (1 point = 5 photo-electrons, i.e. less than the readout noise of 20 electrons). At very low irradiance, for example, ~100 photons per pixel, the signal is strongly affected by the readout noise (20%); but as soon as the signal increases, the signal-to-noise ratio becomes limited by the shot noise (or quantum noise, equal to $\sqrt{N}$, if N is the number of photons collected), for example, ~30 electrons for ~1000 photo-electrons (3% noise). We have verified experimentally the $N/\sqrt{N}$ dependence of the signal-to-noise ratio in the whole dynamic range of the CCD (1000:1, or 60 dB), and observed that the noise could not be decreased much lower than 1% of the signal (at half of the full well capacity, 100 vs. 10000). Unlike the instruments using large area photodiode detectors, where the dynamic range is usually limited by the A/D converter, digital cameras are limited by the full well capacity of the photodiode array. This does not make any difference in the mode of operation of the instruments: to improve sensitivity, the full dynamic range must be used.

Smear effect

The smear effect is a well-known problem associated with CCDs, appearing as a bright vertical stripe emanating from a saturated zone of the array. It persists after the CCD has been overexposed: during the readout process the bright pixels are shifted from the sensor area to the storage area creating a smear on the subsequent image. Our video imaging setup avoids the smear effect because the light pulse used to probe the fluorescence yield is usually more intense than the actinic light (see above). Thus, most often, the actinic light does not cause any artefact. The 250 ms saturating pulse, however, produces a strong burst of fluorescence that may induce a smear effect. This could be minimized in two ways: (i) as the smear effect usually has the same duration as the readout time (~7 ms at full 640 × 480 resolution), increasing the delay between the saturating pulse (~5 ms) and the probe pulse will minimize the artefact while still retaining an accurate reading of F_M and (ii) in order to obtain shorter delays (down to 100 μs), the relative contribution of smear effect could be reduced by an overall increase in signal (increasing the intensity of the probe pulse, and using the full dynamic range of the CCD).

Comparison with other commercially available systems

As described above, the instrument we have built strongly differs from the other PAM systems from Walz (Schreiber et al. 2007) or PSI (Nedbal et al. 2000) companies. The most useful specification of our setup is that the actinic light can be switched off during the measuring light pulse and image acquisition. This allows us to use the full dynamic range of the CCD to probe the fluorescence yield induced by the measuring flash and to reduce the signal-to-noise ratio: we do not need to subtract the background

fluorescence induced by actinic light from the fluorescence induced by the pulse.

Kinetics applications

As described in "Materials and methods" section, flash detection improves time resolution and maximizes the quantity of photons captured by the detector during the exposure time. In our setup, we use a different light source for continuous light excitation and probe pulses. The continuous light is momentarily shut off when the probe pulse is set on the sample. Figure 1 (right panel) shows the time course of the various outputs of the digital delay generator, including continuous light excitation and probe pulse. The pulse generator has 12 TTL programmable outputs (denoted by a letter, from A to L). These TTL outputs are used to trigger the high current power supply, for example, outputs E and F are used to switch on and off the saturating pulse. The excitation light is switched off (H) 20 µs before a detecting pulse is applied (D) and excitation light is switched back on (G) 20 µs after. The exposure time is set by a TTL signal synchronized to the detecting pulse. The readout time, which is the time needed by the CCD to read the pixels, depends on the binning: the larger the binning, the shorter the readout time at the expense of the resolution. The dark intervals (<1 ms) of excitation light are short and sparse enough to have no effect on the actinic effect of the light, which has a much longer duration (seconds to minutes). An additional advantage of the method is that the measured fluorescence yield does not depend on the continuous light intensity, switched off during the measure. Therefore, no normalization is needed to compare fluorescence induction kinetics from various light intensities.

Analysis of cytochrome b_6f mutants

We have tested the sensitivity of our system on the green, unicellular algae *Chlamydomonas reinhardtti* by comparing the wild type strain to mutants deficient or altered in accumulation of the cytochrome b_6f complex. The cytochrome b_6f complex is the chloroplastic plastoquinol–plastocyanin oxido-reductase which transfers electrons between photosystem II and photosystem I. It also participates in the formation of a transmembrane electrochemical proton gradient by transferring protons from the stroma to the lumen. It is minimally composed of four subunits: *cytochrome* b_6, *cytochrome f*, Rieske iron–sulphur protein and subunit IV (SUIV). It has been shown that if one of these components is absent, then the complex will not be assembled in the membranes (Kuras and Wollman 1994) while in unicellular algae PSII, PSI and ATPase will still be accumulated to normal levels. This is the case for the mutant QD3 devoid of SUIV. While it lacks cytochrome b_6f complex, it accumulates normal levels of PSII centres. We have also included the C35V mutant which has a site directed substitution of Cys^{35} to Val preventing thioether bonding of heme c_i (de Vitry et al. 2004) and leading to reduced accumulation of cytochrome b_6f complex (Saint-Marcoux et al. 2009) and the mutants *ini*D1 and *ini*D2. The *ini*D mutants have point mutations in the gene *petD* (encoding SUIV) resulting in a change to the initiation codon ["Initiation codon mutants of *petD*" (*ini*D): *ini*D1 and *ini*D2 carry AUG → AUC and AUG → AUU mutations], leading to inefficient translation, decreased accumulation of SUIV and a weakly phototrophic phenotype (Chen et al. 1993). In Fig. 2, we have verified the accumulation of SUIV and have found it to be in the same range as that reported, being ~10% of wild type levels. Thus, the mutants C35V and *ini*D are useful as examples of less obvious fluorescence phenotypes where electron transfer is less compromised than in a deletion strain.

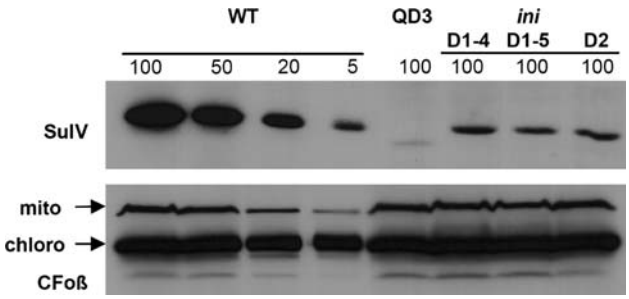

Fig. 2 Western blot showing the quantity of SUIV accumulated in *ini*D strains. The wild type has been loaded at different quantities to estimate the accumulation of SUIV in *ini*D1 and 2. The Cfoß has been included as a loading control

Figure 3 shows the fluorescence induction kinetics (panel A) for streaks of dark-adapted algae (panel B). The sequence used for measuring this response is 3 s of continuous green light (150 µE m^{-2} s^{-1}), a saturating pulse of green light (2100 µE m^{-2} s^{-1}) followed by 4 s of darkness. As described above, the kinetics are not recorded continuously but rather probed by discrete pulses, during the light and dark exposures. The first point of the kinetics is taken in the dark and represents F_0, the first point after the saturating pulse is F_M, and for a better comparison the kinetics are normalized between 0 (F_0) and 1 (F_M). The kinetics curves are plotted for the average signal on 10 × 10 adjacent pixels. The advantage of using probe pulses for the sampling of the fluorescence yield is clear: the maximum frame rate of the camera is used to record the fast fluorescence rise at the onset of illumination, whereas the sampling of images is more sparse when fluorescence reaches its steady state; the initial slope of the post-illumination kinetics is probed at full speed, and the delay

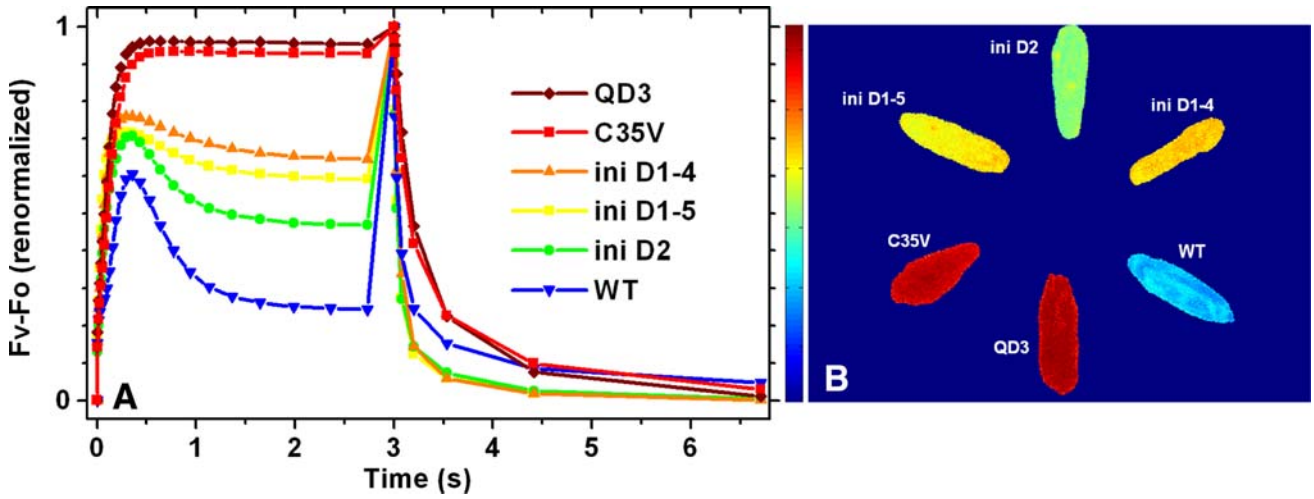

Fig. 3 **a** Induction kinetics of Chlamydomonas (on solid support from panel B) at moderate light (150 μE m^{-2} s^{-1}) with a pulse of saturating light to measure the F_M. **b** A false colour image of labelled strains streaked onto a Petri dish of complete media. The *colour bar* represents the fluorescence level. The animated version of panel B is available as a movie (see Supplementary Material)

between frames is gradually increased. This technique allows an accurate description of the various fluorescence kinetics phases without requiring an excessive amount of memory.

For the wild type, we observe an initial fast fluorescence rise followed by a drop to a steady state level close to F_0. This characteristic transient is linked to limitations on the PSI acceptor side because it is lost when methylviologen is added (MV is an efficient electron acceptor of PSI).

The mutant devoid of cytochrome b_6f complex (QD3) shows a monotonous fluorescence rise to a high stationary value although it does not reach F_M. We have verified that the further increase in fluorescence was not an artefact (see the above discussion on the smear effect). This means that a light intensity of 150 μE m^{-2} s^{-1} is not sufficient to fully reduce the PSII electron acceptor Q_A, and that an additional pulse of 2100 μE m^{-2} s^{-1} is necessary. It is not surprising that saturating light is necessary to reach F_M even in a mutant devoid of cyt b_6f complex. Even if medium light is sufficient to significantly reduce the PQ pool, it may not populate 100% of Q_A^- since charge recombination could compete with charge separation. An alternative and not exclusive explanation is that medium light does not fully reduce the PQ pool because of the activity of the plastid terminal oxidase. We have tested this hypothesis by experiments using cell suspensions treated with saturating concentrations of oxidase inhibitors, 10 mM propylgalate and 10 μM octylgalate (not shown). As expected, the addition of inhibitors results in an increased fluorescence yield but still lower than F_M.

The C35V mutant of cyt b_6f is impaired in heme c_i fixation. This mutation has been reported to allow the assembly of a small quantity of cyt b_6f from residual subunits, as in the case of *ccb* mutants (Saint-Marcoux et al. 2009). Here, we show that the residual amount of cyt b_6f is functional, as the steady-state fluorescence of C35V is measurably less than that of QD3. The three *ini*D mutants show similar fluorescence kinetics, intermediate between QD3 and WT, with a steady-state level of fluorescence correlating with its weakly phototrophic phenotype (Chen et al. 1993). We observe that *ini*D2 appears to be less impaired in photosynthetic electron flow which may be due to a slightly increased accumulation of cyt b_6f complex in this strain, and probably not a drastic change in PSI/PSII stoichiometry because the low amount of cyt b_6f in this strain is limiting for the overall photosynthetic electron flow, even in medium light. These possible changes in cyt b_6f accumulation could be observed by fluorescence kinetics and have not been detected by blot (Fig. 2).

Figure 3 (panel B) shows a false colour image of the labelled strains streaked onto a petri dish of complete media. The colour of the strains represents the steady-state level of fluorescence (F_V) after 2 s of light. Like for the kinetic curves, the variable fluorescence has been normalized and the colour bar shows the fluorescence range from F_0 (dark blue) to F_M (deep red). For ease of comparison, we have used the same colours for the kinetics curves seen in panel A. The streaks show a homogenous steady-state fluorescence F_V, for example, the *ini*D2 streak appears in yellow–green colour, giving a heterogeneity in F_V of $<10\%$ (see colour bar). The different cyt b_6f complex mutants deficient to different degrees can be easily identified and separated on this image.

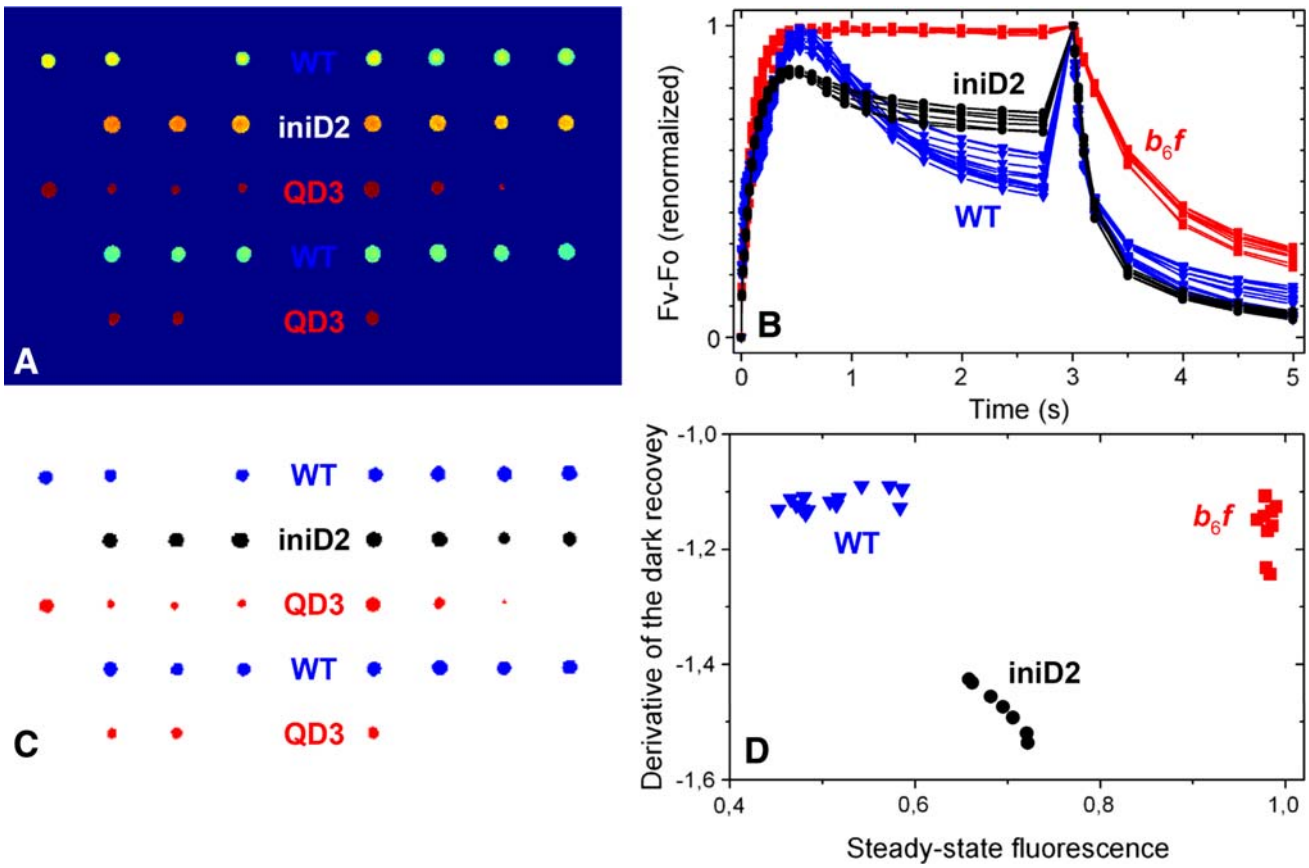

Fig. 4 Localization and representation of multiple colonies. **a** False colour image of F_V, similar to Fig. 3b. **b** Automatic extraction of all kinetics. **c** In-depth clustering of the colonies. **d** Representation in a two-dimensional parameter space, the steady state corresponds to the value before the saturating flash, and the derivative of the dark recovery was calculated on the fifth image after the pulse

Imaging applications

The accuracy of the imaging setup is useful in applications where we screen large numbers of colonies on Petri dishes and where visual information will greatly reduce the time necessary for the screening process.

An illustration of such an application is shown on Fig. 4. Various mutant colonies have been grown on a Petri dish and exhibit different fluorescence behaviours. First, the colonies are automatically localized (Fig. 4a, c) and the associated fluorescence curves are drawn (Fig. 4b). As stated before, this representation makes it easy to separate different mutants: the differences between the steady-state F_V are obvious, and the colony associated with a fluorescence curve can be traced back to the Petri dish in order to be isolated.

However, in-depth analysis can show more subtle clusters. This is achieved through the representation of the fluorescence kinetics in different parameter spaces. Figure 4d shows such a representation: the colonies are plotted as a function of the F_V values at frame 25 (steady state) and the values of the derivatives of their fluorescence curves after the saturating flash. This representation shows three clusters that can be traced back to the fluorescence kinetics and to the colonies on the Petri dish (Fig. 4c). The aim of this procedure is to make screening easier to localize mutants with unusual behaviour. The associated colony will then be taken for further analysis and the mutation identified.

Conclusion

In order to demonstrate the technical abilities of our fluorescence video imaging instrument, in terms of time resolution (<1 ms) and signal-to-noise ratio ($\sim$100), we have chosen to study mutants affected in the assembly of cytochrome b_6f complex, which among the thylakoid proteins has the highest PQ oxidase activity. We have proven that it allows easy discrimination between strains where cytochrome b_6f accumulation is difficult to differentiate by blot (see *ini*D1 and *ini*D2 (Chen et al. 1993)). In Fig. 5, we have represented Q_A and the PQ pool as flared reservoirs with

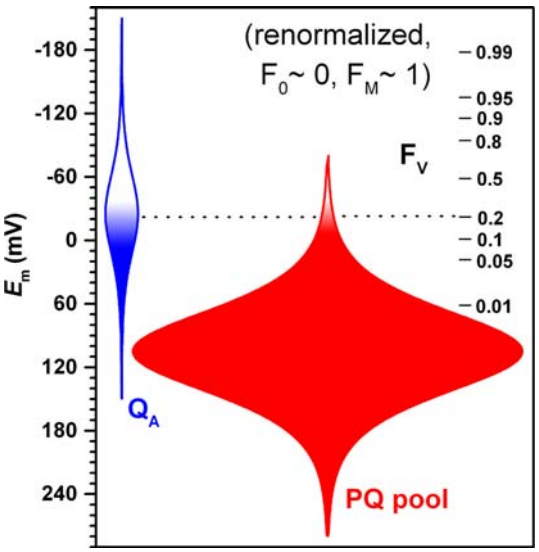

Fig. 5 Schematic representation of the redox equilibration between Q_A and the PQ pool (6 quinones per PSII, i.e. 12 electrons). The steady-state level of fluorescence F_V (nonlinear left vertical scale) corresponding to the population of Q_A^- state is calculated from (Cuni et al. 2004)

areas reflecting their nernstian redox buffering: the overall area of the PQ pool is 12-fold larger than Q_A because the pool contains ~6 quinones per PSII, which are 2-electrons transporters. The nonlinear vertical scale on the left corresponds to the fluorescence signal F_V, normalized between $F_0 = 0$ and $F_M = 1$. It has been calculated from the equation given in (Cuni et al. 2004), which describes the dependence of F_V on the fraction of closed centres c (Q_A^- state) as: $F_V = c/(1 + J - Jc)$, where the parameter J expresses the antenna connectivity of PSII ($J + 1$ being the average number of PSII visited by an exciton when the centre is closed). In Chlamydomonas cells grown under standard conditions, $J \sim 2.6$ (see Cuni et al. 2004). This diagram clearly shows that fluorescence measurements are very sensitive to weak changes in the redox state of the PQ pool, when it is mostly reduced. Indeed, when $F_V - F_0 \sim 0.2 \times (F_M - F_0)$ (see dotted line in Fig. 5), Q_A is approximately half reduced and the PQ pool is filled to more than 99%. Under steady-state illumination, the redox state of the PQ pool depends upon the electron inflow and outflow, the former being dependent upon PSII activity, i.e. light intensity, and the latter being mostly dependent upon cytochrome b_6f activity. Fluorescence measurements at judicious light intensities allow the titration of cytochrome b_6f activity, and may be useful in the screening of mutants accumulating various amounts of this membrane protein.

Acknowledgements The authors are indebted to Catherine de Vitry for the SUIV and CF0ß antibodies and to David Stern for the kind gift of *ini*D mutants. Financial support is acknowledged from Fondation Pierre-Gilles de Gennes pour la recherche and Agence Nationale pour la Recherche ANR-08-BIOE-002 ALGOMICS.

References

Baker NR (2008) Chlorophyll fluorescence: a probe of photosynthesis in vivo. Annu Rev Plant Biol 59:89–113

Bennoun P, Béal D (1997) Screening algal mutant colonies with altered thylakoid electrochemical gradient through fluorescence and delayed luminescence digital imaging. Photosynth Res 51(2):161–165

Bennoun P, Béal D (1998). New digital imaging instrument for measuring fluorescence and delayed luminescence. In: Rochaix J-D, Goldschmidt-Clermont M, Merchant S (eds) The molecular biology of chloroplasts and mitochondria in Chlamydomonas, vol 7. Advances in photosynthesis. Kluwer Academic Publishers, Dordrecht, The Netherlands, pp 451–458

Chen X, Kindle K et al (1993) Initiation codon mutations in the Chlamydomonas chloroplast petD gene result in temperature-sensitive photosynthetic growth. EMBO J 12(9):3627–3635

Cuni A, Xiong L et al (2004) Modification of the pheophytin midpoint potential in photosystem II: modulation of the quantum yield of charge separation and of charge recombination pathways. Phys Chem Chem Phys 6:4825–4831

de Vitry C, Desbois A et al (2004) Biochemical and spectroscopic characterization of the covalent binding of heme to cytochrome b_6. Biochemistry 43(13):3956–3968

Joliot P, Béal D et al (1980) Une nouvelle méthode spectrophotométrique destinée à l'étude des réactions photosynthétiques. J Chim Phys 77(3):209–216

Kuras R, Wollman FA (1994) The assembly of cytochrome b6/f complexes: an approach using genetic transformation of the green alga *Chlamydomonas reinhardtii*. EMBO J 13(5):1019–1027

Nedbal L, Soukupova J et al (2000) Kinetic imaging of chlorophyll fluorescence using modulated light. Photosynth Res 66(1–2): 3–12

Saint-Marcoux D, Wollman F-A et al. (2009) Biogenesis of cytochrome b_6 in photosynthetic membranes. J Cell Biol 85(7):1195–1207

Schreiber U, Quayle P et al (2007) Methodology and evaluation of a highly sensitive algae toxicity test based on multiwell chlorophyll fluorescence imaging. Biosens Bioelectron 22(11):2554–2563